American Journal of Climate Change, 2025, 14(1), 119-145
https://www.scirp.org/journal/ajcc
ISSN Online: 2167-9509
ISSN Print: 2167-9495

Atmospheric Dynamics of Extreme Precipitation over the West African Sahel

Mouhammed Fall[1*], Abdou L. Dieng[1], Laurence Eymard[2], Gaëlle De Coëtlogon[2], Saidou M. Sall[1], Youssouph Sane[3]

[1]Laboratoire de Physique de l'Atmosphère et de l'Océan-Siméon Fongang (LPAO-SF), École Supérieure Polytechnique, Université Cheikh Anta Diop, Dakar, Sénégal
[2]Laboratoire Atmosphère et Observations Spatiales (LATMOS), Sorbonne Université, Paris, France
[3]Agence Nationale de l'Aviation Civile et de la Météorologie (ANACIM), Dakar, Sénégal
Email: *mouhammed.fall@ucad.edu.sn

How to cite this paper: Fall, M., Dieng, A. L., Eymard, L., Coëtlogon, G. D., Sall, S. M., & Sane, Y. (2025). Atmospheric Dynamics of Extreme Precipitation over the West African Sahel. *American Journal of Climate Change, 14,* 119-145.
https://doi.org/10.4236/ajcc.2025.141007

Received: January 23, 2025
Accepted: March 24, 2025
Published: March 27, 2025

Abstract

The period of the 70s and 80s was marked by a drought in the Sahelian countries. However, since the beginning of the 21st century, these countries have experienced a resurgence of heavy rainfall and devastating floods, causing inestimable socio-economic damage and losses. The objective of this work is to study the dynamics of atmospheric conditions associated with seventeen extreme rainfall events listed in the database of the Directorate of Civil Protection of Senegal and having caused significant socio-economic impacts between 2000 and 2017. This study was carried out using satellite products and atmospheric reanalysis data. The results of the analyses of the various atmospheric parameters studied show, at the synoptic scale, that extreme rainfall events are mainly modulated by African easterly waves. Strong moisture transport convergences in the lower tropospheric layers due to vortices associated with these waves are recorded. A response of this moisture convergence in the lower layers accompanied by vertical moisture transport is highlighted by strong anomalies and wind divergence. This configuration corresponds to the presence of a vertically well-structured convective system. The analysis of atmospheric parameters such as relative vorticity, wind, relative humidity and precipitable water shows that they are good indicators to characterize rainfall extremes. The behavior of the anomalies of these variables shows the presence of a significant amount of moisture in the tropospheric column and the most marked pressure levels are between 850 and 700-hPa, and in the upper layers around 200-hPa.

Keywords

Extreme Rainfall Events, Convective Systems, African Easterly Waves, Climate Dynamic, Climate Change, Climate Impacts

1. Introduction

In West Africa, the Sahelian strip is one of the regions of the world where climatic extremes are more marked. The rainfall evolution in the Sahel, during the second half of the 20th century, is characterized by two clearly marked periods: a wet one, between the 50s and 60s, and a dry one from the 70s to the mid-1990s. The period drought, corresponding to the most intense and longest ever recorded in the world (Hulme et al., 2001; Dai et al., 2004). However, between the end of the 1990s and the beginning of the 21st century, the Sahelian countries experienced a return to normal precipitation regime conditions (Le Barbé et al., 2002; Bell & Lamb, 2006; Lebel & Ali, 2009; Descroix et al., 2016). The latter is particularly marked in the western Sahel with strong variability in precipitation, dry breaks and the length of wet seasons (Salack et al., 2011, 2016; Ly et al., 2013). Even if the average annual level of precipitation remains lower than the average observed over the entire 20th century (Lebel & Ali, 2009; Gallego et al., 2015), an increase in extreme events is one of the main phenomena (Panthou et al., 2014, 2018; Descroix et al., 2016; Wilcox et al., 2018). The studies by Taylor et al. (2017) based on observations in the Sahel, showed that extreme rainfall events have become more numerous than during the period of the 1950s and would be positively correlated with the climate change signal. Sanogo et al., 2015 showed a significant increase in daily precipitation above the 95th percentile across the Sahel and the Guinean coast over the period 1980-2010. These events could amplify and become more frequent in this context of climate change.

In the Sahel, urban areas are particularly vulnerable to flooding. Several studies (Hardoy, 2001; Nchito, 2007; Douglas et al., 2008) have shown insufficient urban planning which exposes these poor settled populations. These heavy rain phenomena also cause inestimable damage and socio-economic losses with human and material losses, diseases, poor harvests, etc. All these parameters contribute to the decline in the availability of human resources and the inaccessibility of basic necessities, thus leading to speculation in foodstuffs (Hartill, 2008). As a result, populations are exposed to increased food insecurity and climate migration.

Faced with the challenges posed by these phenomena and the uncertainties of climate simulation models (Wang et al., 2014; Siongco et al., 2015), improving our knowledge of the atmospheric conditions associated with extreme rainfall is becoming a major concern for the scientific community and meteorological services. To address these issues, the main question remains what determines the predictability of these events. Precipitation in West Africa is modulated in intensity by African Easterly Waves (AEW) with estimates suggesting that more than 60% of squall lines, during the monsoon period, are associated with AEW (Fink & Reiner, 2003). Crétat et al., 2015 analyzed the relationship between daily precipitation and AEW, at a regional scale, in West Africa. They concluded that 3-to-5-day AEWs establish the most favorable synoptic conditions for the development of intense rainfall events. Mesoscale Convective Systems (MCS) are integrated into AEWs which are synoptic disturbances of wavelength of the order of 3000 - 4000 km and

which propagate westward at 6 - 7 $m \cdot s^{-1}$. AEWs feed MCSs with vorticity (Schwendike & Jones, 2010; Berry & Thorncroft, 2012) and moisture (Poan et al., 2015). The availability of humidity is by far the limiting factor in convective activity over the Sahel. This explains why MCS develops over the Sahel during the summer season when sufficient moisture is available in the region. Moisture is mainly brought into the lower layers of the atmosphere (surface-850 hPa) by the southwest monsoon flow.

Therefore, several fairly recent studies have focused on the characteristics of extreme daily precipitation types in the Sahel and have highlighted the influence of AEW and its moisture supply (Cornforth et al., 2017; Engel et al., 2017; Lafore et al., 2017; Vischel et al., 2019; Fall et al., 2020; Vizy & Cook, 2022, 2024). However, most generally rely on isolated case studies (September 1, 2009 in Ouagadougou and August 26, 2012 in Dakar), making any generalization difficult. In addition, the occurrence of an extreme rain event can involve several phenomena of different spatiotemporal scales (Lafore et al., 2017). For this it is necessary to carry out several individual case studies but also composite ones with statistical tests. For this, Vischel et al., 2019 performed a composite analysis of the 20 most extreme rainfall events in Ouagadougou since 1997. They found the association of synoptic (AEW) and large-scale (wet anomaly) atmospheric factors. However, there is not yet a composite study covering extreme rain events in several different locations in the western Sahel and in particular in Senegal.

The main objective of this paper is to study the atmospheric conditions associated with extreme rain events listed in the database of the Directorate of Civil Protection of Senegal (DPC) and having caused significant socio-economic impacts. On the one hand, the analyzes will make it possible to characterize the atmospheric dynamics of extreme rain events on different spatio-temporal scales. On the other hand, highlight the main atmospheric signals associated with this type of event in order to propose indicators that can help in their prediction.

The paper will be structured as follows. After presenting the data and analysis methods in section 2, the results obtained thanks to satellite observations and reanalysis data will be presented in section 3. Based on these results, discussions are made in section 4.

2. Data and Methods

2.1. Data

The Directorate of Civil Protection (DPC) is attached to the Ministry of the Interior and Public Security of Senegal and is responsible for the prevention of risks of all kinds, as well as the protection of people, property and the environment against all disasters. The DPC reports made it possible to identify, between 2000 and 2017, the 17 extreme weather cases analyzed in this study.

The daily data used as references to quantify precipitation come from the National Agency for Civil Aviation and Meteorology of Senegal (ANACIM). The rainfall stations, present at the locations where the events took place (**Figure 1(b)**),

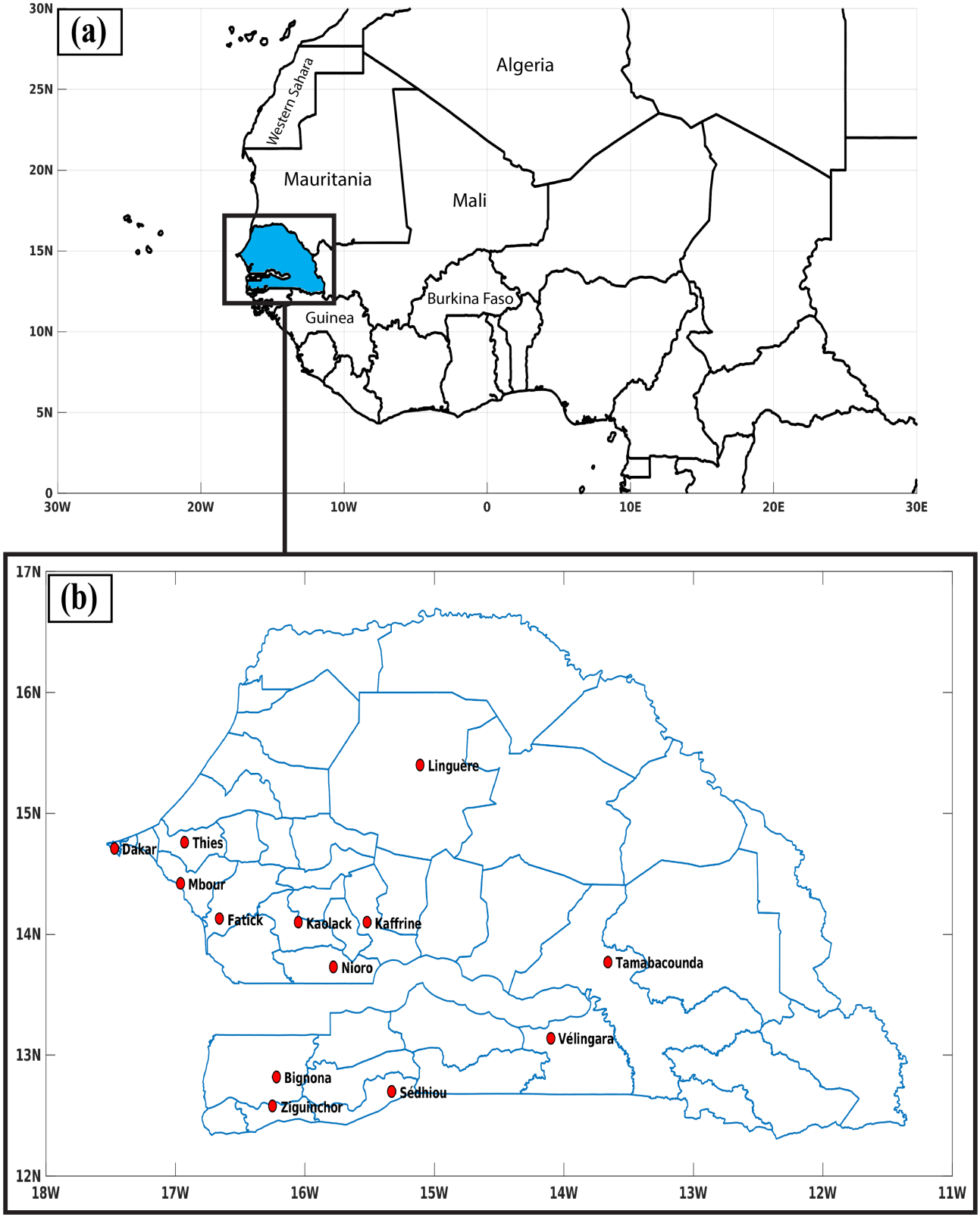

Figure 1. (a) West Africa, Senegal is indicated by the blue zone. (b) Map of Senegal. The red dots represent the geographic positions of areas affected by extreme rain events.

were used to evaluate the associated rainfall quantities.

The TRMM mission (Tropical Rainfall Measuring Mission) is a joint mission between the American (NASA) and Japanese (NASDA then Jaxa) space agencies which operates a satellite in equatorial orbit for the observation of precipitation in the tropical band between 30˚N and 30˚S. It therefore has a high repeatability over West Africa with around 8 passages per day. Temporal and spatial measurement of precipitation variations is essential to understanding global weather phenomena. The data collected by TRMM are essential for understanding the tropical climate and its evolution. The project was launched on November 27, 1997 with the Visible and Infrared Scanner (VIRS; 5 channels), the TRMM Microwave Imager (TMI; 9 channels), and the Precipitation Radar (PR) (Huffman et al., 2007). Nicholson et al., 2003 evaluated TRMM products over West Africa during the monsoon season and showed excellent agreement with station data. The studies of Maggioni et al., 2016 highlight the superiority of the TRMM 3B42 V6 over other SRFEs from East and West Africa on a daily scale and at 0.25˚ spatial scale. Knowing that Zulkafli et al., 2014 and Prakash et al., 2015 provided evidence that V6 and V7 are rather comparable, so version 7 of the 3B42 dataset is used in this study for spatial monitoring of precipitation. It provides a 3-hour precipitation estimate on a 0.25˚ grid.

The 4 km merged IR Brightness Temperature (BT) data is produced by the Climate Prediction Center (CPC) of NOAA's National Environmental Prediction Center. Each cooperating geostationary (geo)satellite operator (Geosynchronous Operational Environment Satellites (GOES), USA, Geosynchronous Meteorological Satellite (GMS), followed by Multifunctional Transport Satellite (MTSat), then Himawari, Japan, and Meteorological Satellite (Meteosat) (European Community) transmits infrared (IR) images to the CPC. Then, the global geo-IRs are corrected for zenith angle (Joyce et al., 2001), redirected for parallax and merged on a global grid. In case of data duplication within a grid, the value with the smallest zenith angle is taken. The data are provided on a 4 km equivalent latitude/longitude grid on the 60˚N-S latitude band, and its temporal resolution is 30 minutes.

ERA5 is the fifth major global reanalysis produced by ECMWF (European Center for Medium-Range Weather Forecasts). Data processing is done using the IFS (Integrated Forecast System) model of the ECMWF Earth system, cycle 41r2. ERA5 combines large quantities of historical observations into global estimates using advanced modeling and data assimilation systems. ERA5 replaces the ERAI reanalysis which ceased production on August 31, 2019. ERA5 data are available on regular latitude-longitude grids at 0.25˚ resolution, with atmospheric parameters over 37 pressure levels. The temporal resolution of this reanalysis is one hour. Studies by Hersbach et al., 2020 have shown that these data represent the state of the atmosphere quite well.

2.2. Methods

Starting from the chosen space, the composite analysis makes it possible to

characterize the average state of a phenomenon from a set of events typical of this phenomenon. In this study, direct calculation without calibration is applied to large-scale composites (0 - 30˚N and 0 - 30˚W). Knowing that the positions of the places where the events took place are not located on fairly close latitudes and longitudes (see **Figure 1(b)**), the direct calculation of the composites without taking this contrast into account could have an effect on the structure of the composite signals. To overcome this problem, the method used by Reed et al., 1977 is adopted using a relative benchmark centered on each location affected by the extreme rainfall. Then, the data fields are averaged around these positions to have the corresponding composite structures. The composite obtained is thus centered around two positions: the reference longitude (Xref 0) and the reference latitude (Yref 0). The reference date is thus considered to be the time closest to the actual date on which the precipitation began and this date is called H00. Composite analysis has been used in several studies (Lamb, 1978a, 1978b; Janicot, 1992a, 1992b; Hastenrath, 1999) to characterize rainfall structures in West Africa. From this approach, a diagnosis of several atmospheric parameters at different tropospheric pressure levels and at different time scales in the short term is made.

To physically interpret the composite, it is first necessary to verify the statistical significance of the composite. Otherwise, it is necessary to ensure that this average is not zero statistically speaking and can therefore be interpreted physically. For this, the Monte Carlo significance test is used. It is applied, for several atmospheric variables studied, considering the 90th percentile as a significance threshold. The number of random composites used for this test is 1000 experiments.

A comparison of the structures obtained from the rainfall extremes is made with those of the composite of moderate rainfall events. The dates of moderate rainfall events are obtained by calculating the interval between the 60^{th} and 70^{th} percentiles with TRMM and they are validated with ground data. The locations and number of dates do not change with 17 moderate rainfall cases as with extreme rainfall, and the same year and month are considered for each comparative case.

The anomaly used in this work is calculated in relation to a duration of 31 days centered on the day in question, that is to say for each date, a difference in the value of the variable between this date and the average of the 15 days before and 15 days after. These anomalies allowed us to characterize the profound changes in atmospheric conditions which favored or caused the events. They also allow us to take into account the intra-seasonal effect which will not influence this anomaly.

3. Results and Discussions

3.1. Horizontal Structure

3.1.1. The Precipitations

Figure 2 represents the Hovmoller diagram of the composite of hourly precipitation extremes with TRMM and its significance between H-72 to H+72. The analysis already shows the presence of rain around the reference longitude Xref 0 between H-72 and H-48. However, a second more intense rain is noted around H00

with a maximum intensity which is significant (between 2 and 3.5 mm·h^{-1}) between H00 and H+06 fairly localized around Xref 0. The propagation of precipitation in function of time is from East to West, which brings us back to the large MCS which represent up to 90% of total precipitation in the Sahel (Lebel et al., 2003).

The composite analysis of Figure 3, which represents the brightness temperature

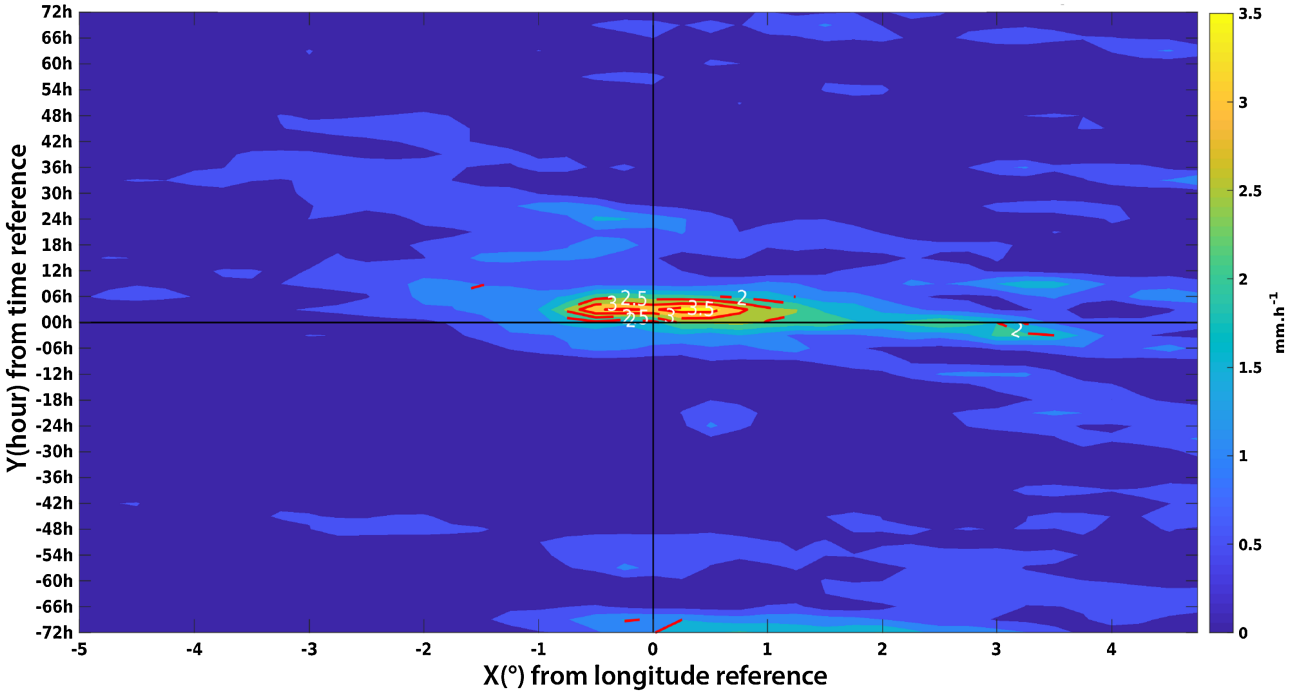

Figure 2. Hovmoller diagram of the precipitation composite (color) and its significance (isoline) with TRMM. The vertical black line is the reference longitude and the horizontal black line is the reference time for the start of precipitation.

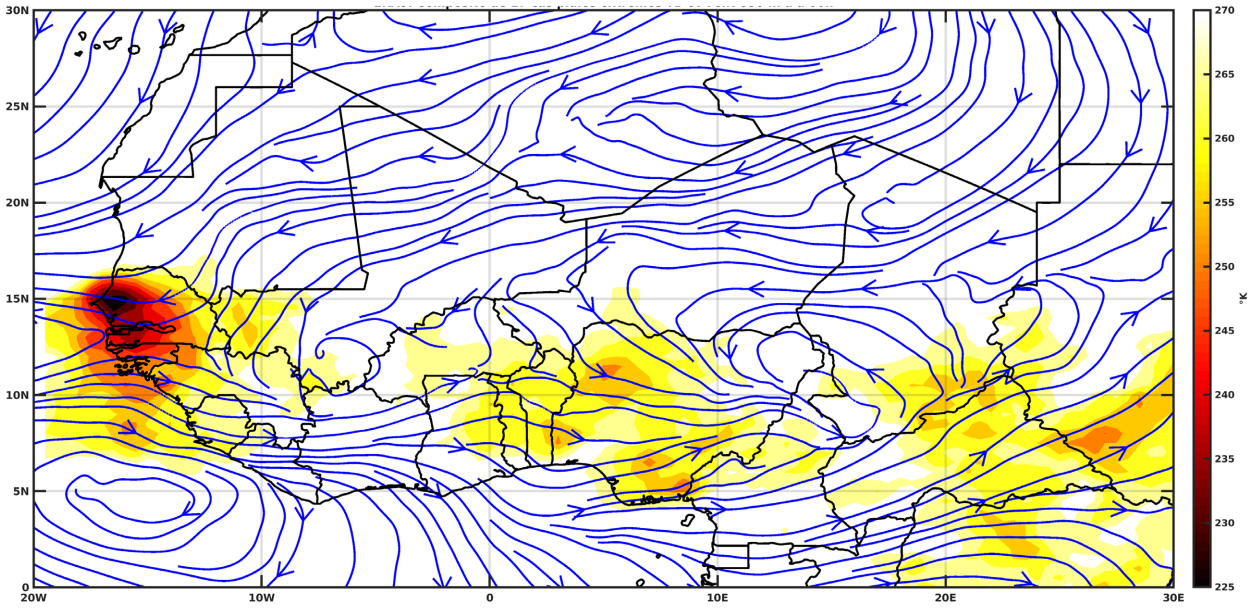

Figure 3. Composite of brightness temperature and wind at 850-hPa.

and the wind at 850-hPa at H00, indicates that the precipitating convective system is located ahead of the wave trough, which is consistent with several studies of observations which concluded that deep convection tends to occur in front of the wave trough (Carlson, 1969a, 1969b; Payne & McGarry, 1977; Reed et al., 1977; Diedhiou et al., 1999; Kiladis et al., 2006).

An analysis of the vorticity relative to 700-hPa is carried out in order to see a possible position of the AEWs in relation to the precipitation linked to extreme rain events (EEP). This choice of pressure level makes it possible to detect possible AEW as well as the Thalweg associated with the wave (Fink et al., 2006; Kiladis et al., 2006; Berry et al., 2007; Bain et al., 2014). A comparison is also made with moderate rain events (EPM) in order to highlight the differences in their structures.

Figure 4 shows the Hovmoller diagram of the composite of 700-hPa relative vorticity (in color) with ERA5 and precipitation with TRMM (in isolines) for EEP (**Figure 3(a)**) and EPM (**Figure 3(b)**). For the EEPs, the propagation of two relative vorticity disturbances is listed. A first less intense (2×10^{-5} s^{-1}) which passes around Xref 0 between H-72 and H-48 and a second with a more marked intensity (4×10^{-5} s^{-1}) from H00. Each of these two disturbances gave rise to precipitation proportional to its intensity.

In comparison with the EPMs, the analysis highlights two different configurations in terms of spatialization and intensity. Extreme rainfall is characterized by an east-west propagation of precipitation over time, while for moderate rainfall a localized effect of precipitation over time and intermittently is noted. Just like the extremes of rain, the moderate ones present a positive relative vorticity which propagates from East to West. However, its maximum value is 1.5×10^{-5} s^{-1}, or half as intense as that obtained with the extremes of rain (4×10^{-5} s^{-1}).

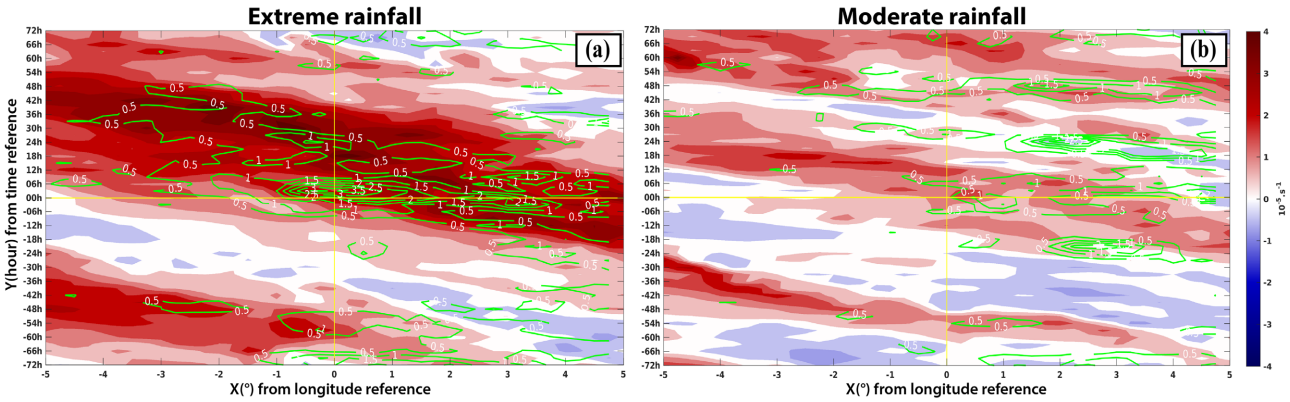

Figure 4. Hovmoller diagram of the composite of relative vorticity at 700-hPa (color) with ERA5 and precipitation with TRMM (isoline). Left for extreme rain (a) and right for moderate rain (b). The vertical yellow line is the reference longitude and the horizontal yellow line is the reference time for the start of precipitation.

3.1.2. Influence of AEW

In West Africa, the AEWs are more marked in the lower troposphere with a maximum at the AEJ level. Carlson (1969a, 1969b) studied the synoptic structure of several observed AEWs, and noted the presence of wave disturbances of the 700-

hPa wind field. Having detected the presence of waves modulating the extremes of rainfall, an analysis on a larger scale is carried out in order to have a better spatial vision of the signals.

Figure 5 shows the behavior of relative vorticity, wind and RH at 700-hPa at H00. It shows that the direction of the AEJ is established following the trajectory of the maximum relative vorticity and the retroactivity of these latter modules well with the presence of a fairly considerable quantity of relative humidity (>65%) at the same pressure level. The main signal for the EEPs (Figure 5(a)) is the position of the relative vorticity maximum with respect to the EPMs (Figure 5(b)). For the EEP, the maximum is located around Senegal and north of Guinea (between 10 and 17˚N) with values reaching 4×10^{-5} s^{-1}, while for the EPM its location is only north of Guinea (between 8 and 16˚N) with a maximum vorticity of 2×10^{-5} s^{-1}. This configuration is reflected in the positions of the maximum HR values which are further north for the EEPs than for the EPMs.

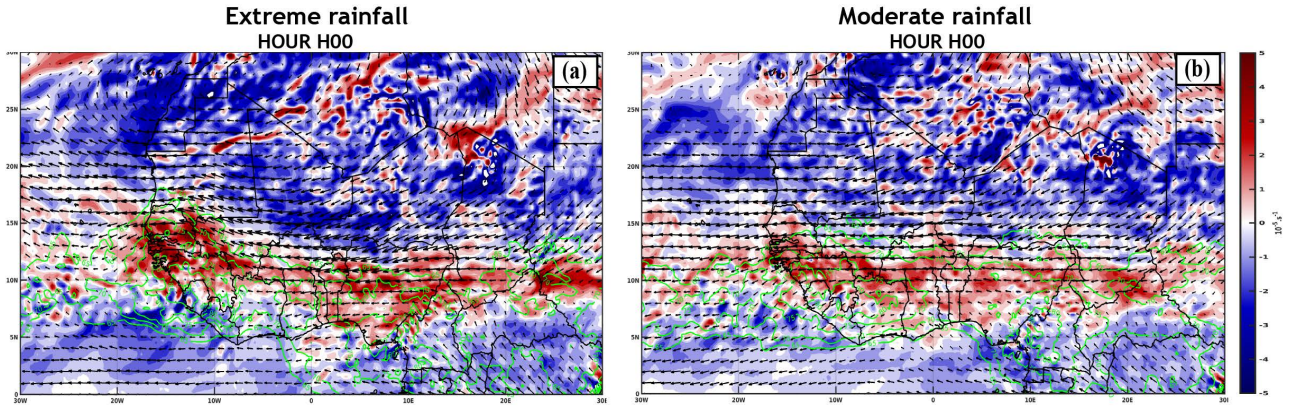

Figure 5. Composite of relative vorticity (color), wind (arrows) and relative humidity (>65% in isolines) at 700-hPa. (a) represents extreme rain events and (b) those of moderate rain at H00.

The analysis of wind anomalies, relative vorticity and its significance at 700-hPa (Figure 6) shows, at H-48, strong wave activity with two main troughs. One is located at the level of the cyclonic circulation (C1) which is on the Senegalese-Mauritanian coast (between 15˚N - 20˚N) and the other (C2) on the continent around the area between Mali and Burkina Faso (between 10˚N - 15˚N). These disturbances are also accompanied by significant relative vorticity anomalies. At H-24 the two cyclonic circulations (C1 and C2) progress towards the West and between the two we note an anticyclonic circulation (A) of the wind anomaly corresponding to the ridge of the wave. From H-12, the center of the continental cyclonic circulation (C2) arrives over Senegal and its position becomes more northerly. This configuration can explain the deviation of the AEJ's trajectory towards the North-West over Senegal (see Figure 5 with the raw wind at 700-hPa).

Another vorticity anomaly with a cyclonic circulation (C3) is noted between 20 and 25˚N. It could be compared to the dry convection linked to the Saharan depression. Its movement also occurs, throughout the process, from East to West and would seem to be coupled to the C2 vortex.

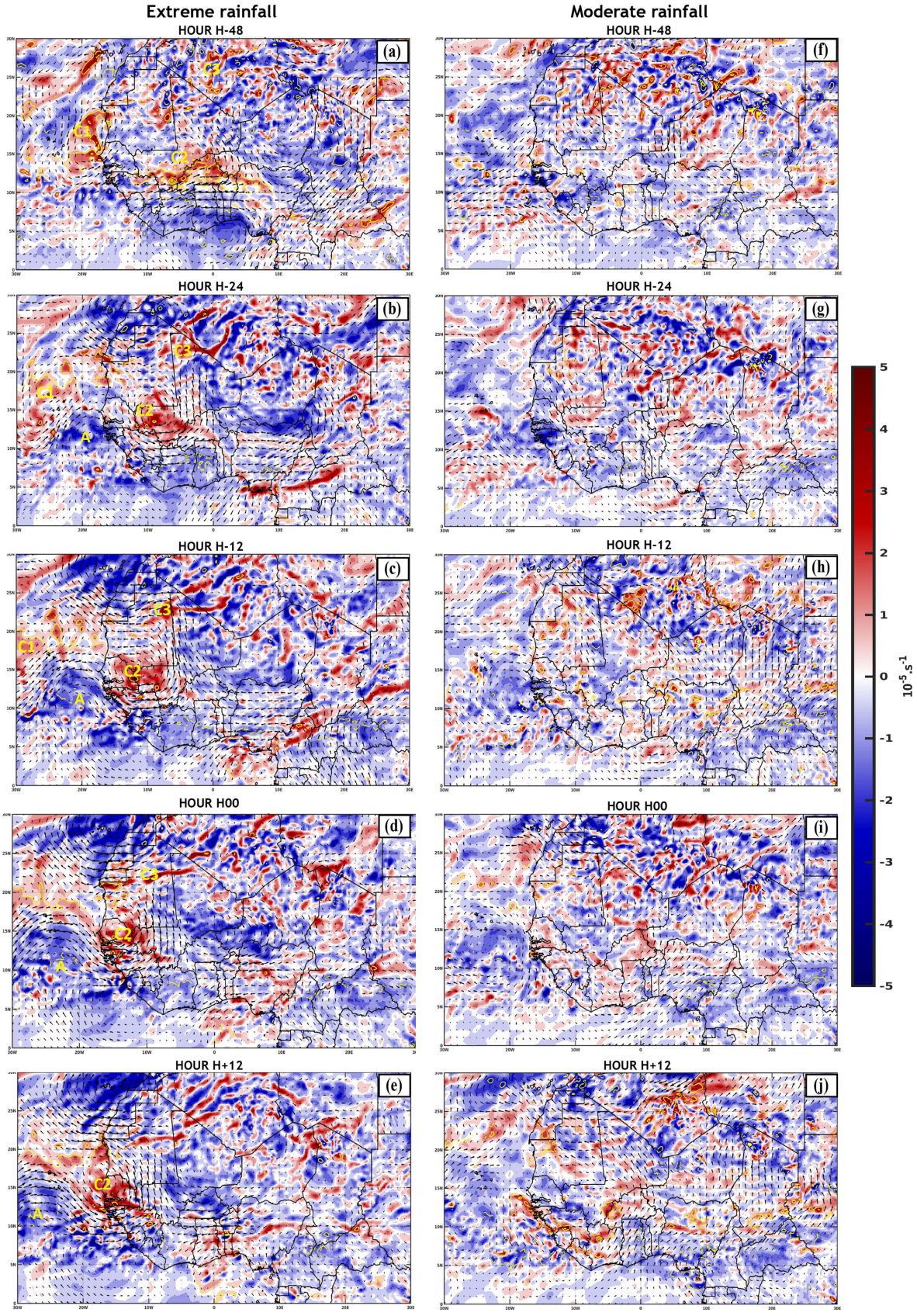

Figure 6. Anomalies of wind (arrows) and relative vorticity (color) and its significance at 700-hPa.

In comparison with the EEP, the configuration of the same variables in anomalies for the EPM does not indicate any particular signals except a fairly localized anomaly of the RH around the southwest of Mali and Mauritania (around between 5˚W - 10˚W and 12˚N - 17˚N). The positive relative and significant vorticity anomaly, corresponding to the cyclonic wind circulation, is noted at H+12 and is located in the southwestern part of Senegal including the eastern part of the Atlantic coast.

3.1.3. Moisture Supply in the Tropospheric Layer

MCSs are closely related to low-level synoptic disturbances caused by AEWs (Fink & Reiner, 2003). The structure of moisture transport in the low levels is important for the delivery of moisture to the continental surface. **Figure 7** shows anomalies of moisture transport, its divergence and integrated moisture between the surface and 850-hPa.

The arrangement of the two main vortices of the moisture transport anomaly is quite similar to that of the 700-hPa wind anomaly (see **Figure 6**). The first cyclonic circulation (C1) is found in the ocean and the second (C2) on the continent even if their spatial positions are more offset from the 700-hPa wind anomaly (about 5˚ to the West). Between H-48 and H-24, these vortices progress towards the West and a transport anomaly from the South-West to the South is noted on the ocean off the Senegalese-Mauritanian coasts generating a humidity anomaly around 20˚N. Around H-12 we note the strengthening of the ridge of the wave creating an anticyclonic circulation (A) near the coasts generating a transport anomaly of humidity from the sea towards the continent and thus reinforcing in terms of humidity the west face of the cyclonic circulation located on the continent (C2). Between H00 and H+12, the cyclonic circulation accompanying the precipitating convective system (C2) intensifies with a convergence of humidity and covers all of Senegal as well as the area surrounding it.

In comparison with the EEP, the EMP composite also presents a southerly transport off the Senegalese-Mauritanian coasts at H-24, part of which is redirected towards the continental surface. However, between H00 and H+12 we note a cyclonic circulation which is not as closed as with the EEP composite and its position is below the positive relative vorticity anomalies listed (**Figure 6(i)**).

In terms of precipitable water anomalies in the low layers, for the two types of events (EEP and EMP) the main signal is the presence of humidity in the north of Senegal on the continental west side and at the level of the East of the Atlantic Ocean at the same latitude (between 15˚N and 25˚N).

In particular the EEPs are characterized by a strong convergence of humidity due to the vortices of the wave. This humidity is more marked in the North because the ridge (which is located around 20˚W and 15˚N at H-24) has transported a lot of humidity to the North of Senegal. However, it should also be noted that the second cyclonic circulation (C2) accompanying the event also advected humidity, coming from off the Guinean coast and a little further south, towards the continental North between Mali and Mauritania. This arrangement

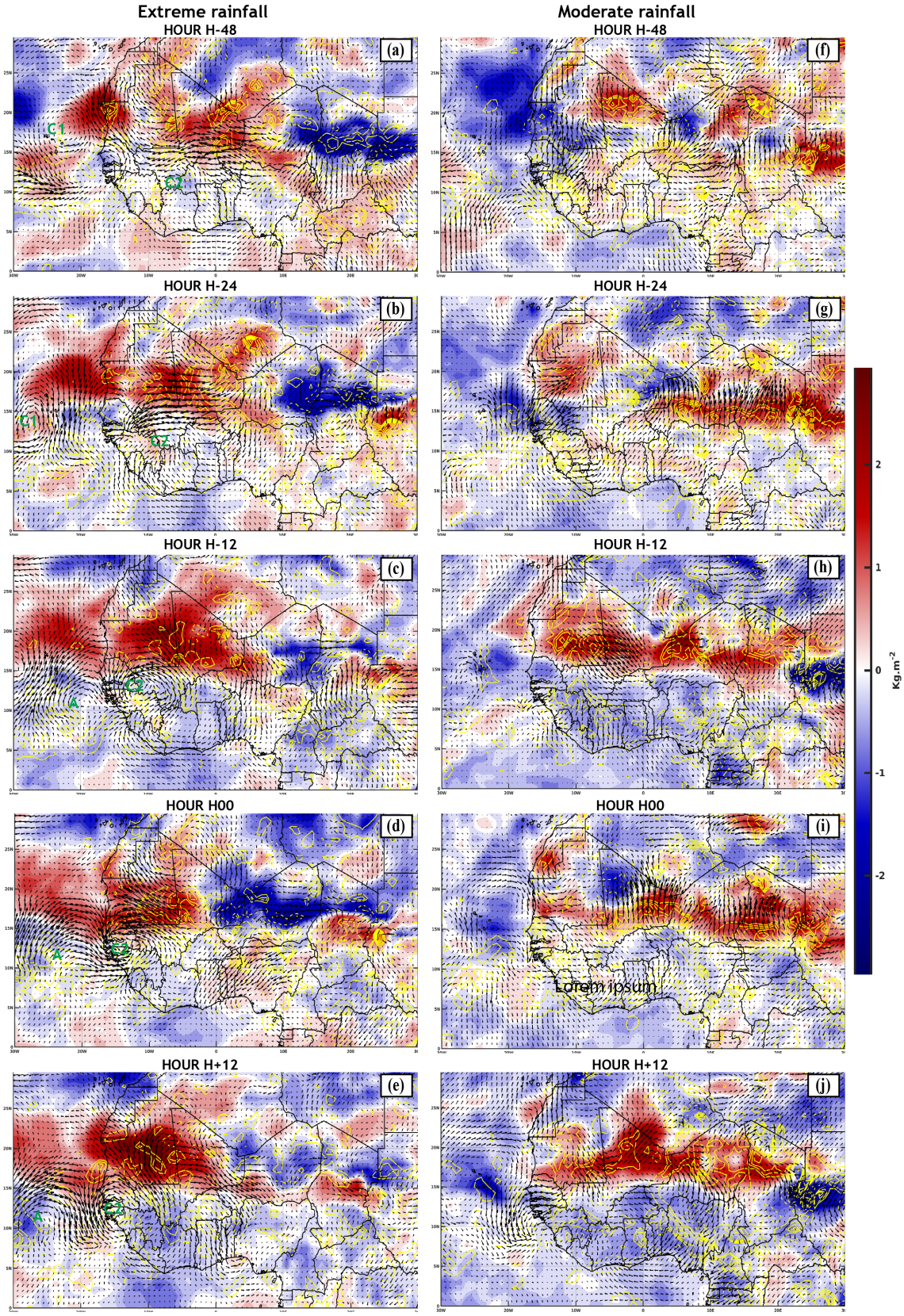

Figure 7. Anomalies of moisture transport (arrow), its divergence (isolines) and integrated humidity (colors) between the surface and 850-hPa.

corresponds to the studies of (Crétat et al., 2015) which show that the AEW establishes a transport of moisture towards the north between the trough and the ridge.

After observing the activity of the moisture flux in the lower layers, a complementary analysis is carried out in the upper layers of the atmosphere. **Figure 8** is composed of wind and relative humidity anomalies at 200-hPa. The main signal noted at H-24 in southwest Mali with a strong humidity anomaly. Around H00 the latter is centered on Senegal with a maximum value of 25% and continues its progression towards the West at ocean level around H+12. We also note a similar signal in Senegal for EMPs, however it is less marked. For the wind anomaly, a strong divergence is noted between H00 and H+12 for the EEP while this is not the case for the EPM. Just like the configuration of the integrated moisture transport anomaly in the low layers, we note a progression from East to West of the relative humidity anomaly as well as the divergence of the wind at 200-hPa for the EEP.

Convergence in the low levels induces divergence aloft through vertical transport of moisture, indicating conditions conducive to the development of deep convection thus giving a well-structured vertically precipitating cloud system.

3.1.4. The SHL

Zhang et al., 2006 showed, based on observations, that the ITCZ is influenced by two meridional flows: the African monsoon, between the surface and around 850-hPa, and a northerly flow around 700-hPa. It was suggested that the latter would be associated with the Saharan Hit-Low (SHL). The position of the SHL as well as its intensity plays an important role in the dynamics of the African monsoon because it largely modulates the intensity and direction of the moisture flow in the Sahel. **Figure 9** shows the composite of Mean Sea Level Pressure (MSLP) and 925-hPa wind at H00. There is a difference in relation to the position of the closed wind circulation (defined here as the center of the SHL) as well as the intensity of the surface pressure. For the EEP (**Figure 8(a)**) the position of the center of the SHL is over Mauritania around 20˚N with a pressure between 1007 and 1008-hPa while for the EPM (**Figure 8(b)**) its position is between the border between Mauritania and Mali around 23˚N with an intensity of 1006-hPa.

To analyze the associated regional and synoptic-scale climate signals, Lavaysse et al., 2009 focused on the intra-seasonal pulsations of the SHL. A spectral analysis showed the existence of two significant pulsation periods: from 3 to 10 days and from 10 to 30 days. The short period pulsations are associated with the advection of moist and cold air masses in the lower levels, caused by the passage of an East African Wave, while the longer period pulsations are associated with the passage large-scale waves over the Mediterranean.

Knowing that AEWs are present in this present study, the calculation of surface pressure and wind anomalies at 10 m here is done by considering 11 days centered on D-Day and the diurnal cycle does not influence this calculation. These anomalies are represented in **Figure 10** in order to see the profound modifications

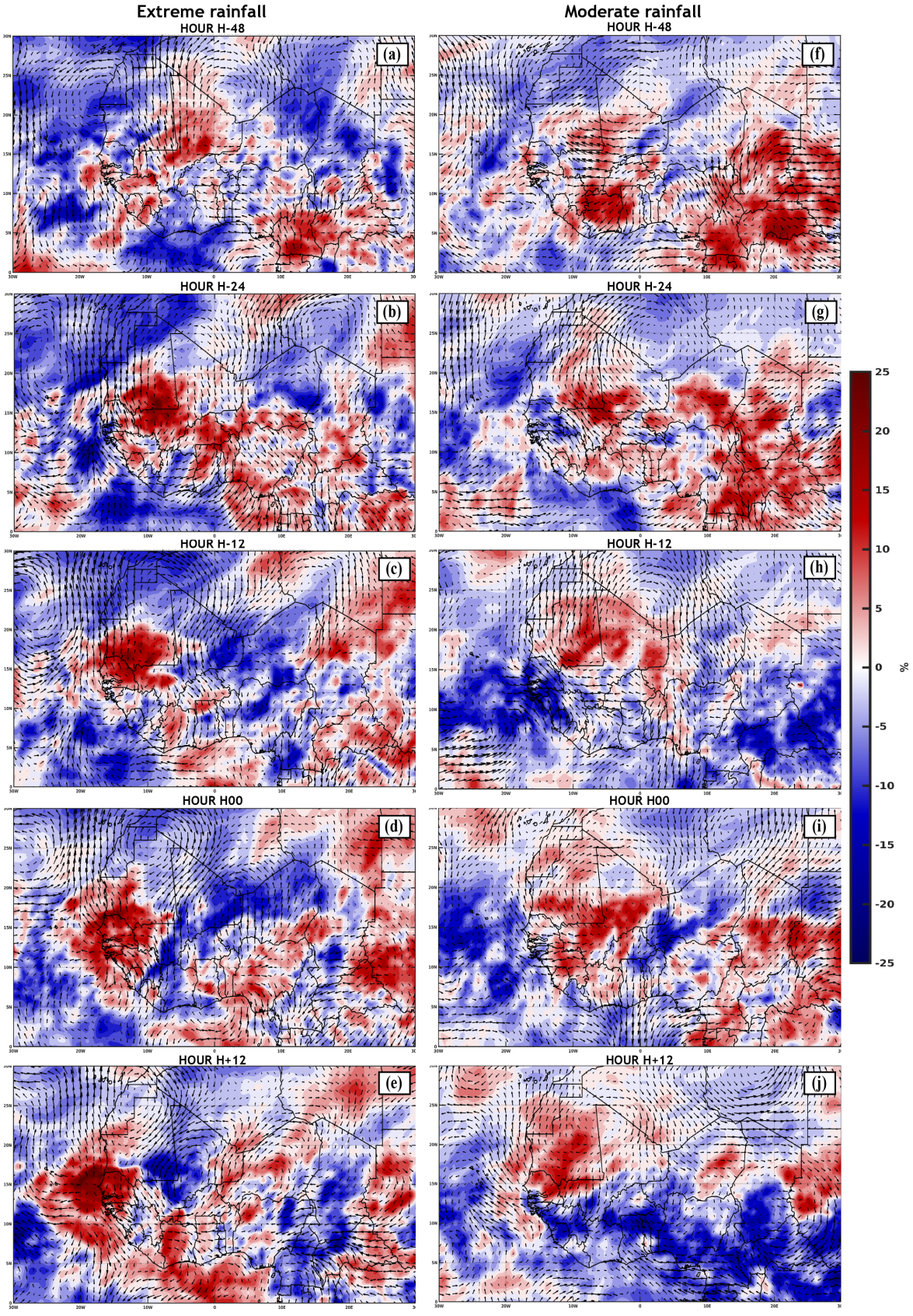

Figure 8. Anomalies of relative humidity (colors) and wind (arrows) at 200-hPa.

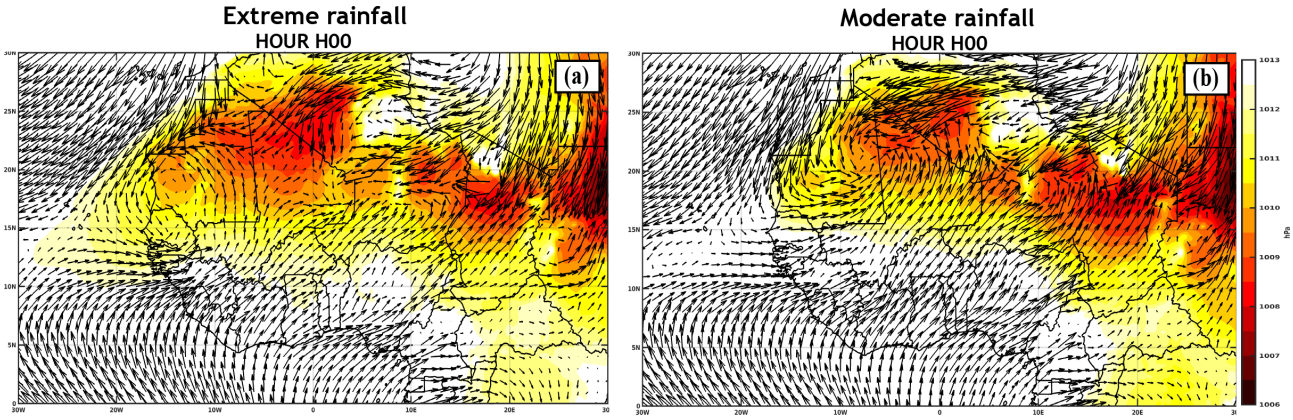

Figure 9. Mean sea level pressure (color) and wind at 925-hPa (arrows).

linked to the SHL for EEPs in comparison with EMPs. At H-48, for both types of events, we have positive pressure anomalies at the position of the SHL (yellow circle), previously described with the raw pressure minimum (**Figure 9**). It is from H-24 that a remarkable difference is noted with a negative anomaly for the EPM composite (**Figure 10(g)**) whose maximum is found between Niger, Mali and southern Algeria (green circle). For the EEP (**Figure 10(b)**) the anomaly remains positive near this area and its maximum is located around north-central Mali. This arrangement of these anomalies, for both types of events, is maintained throughout the processes with a slight shift of the anomalies towards the West.

Aside from the signal around the SHL, between H-12 and H+12, the EEP composite in particular shows two main signals. On the one hand a negative anomaly around Senegal which marks the signal of the passage of the wave trough (C2) accompanying the convective systems and on the other hand a positive anomaly at sea level off the Senegalese Mauritanian coasts, corresponding at the backbone of the wave (A).

EPMs are accompanied by a more intense SHL than EEPs and the position of the SHL influences the direction of moisture flux transport. However, a positive surface pressure anomaly is noted, so the intensity of the SHL may not play an important role in the intensity of the moisture flux at the continental level. The presence of high humidity values at the continental level during the EEP can be attributed, in large part, to the passage of the wave with the cyclonic circulation under which a surface depression which accompanies the precipitating system is located.

3.2. Vertical Structure

The results on the horizontal structures of humidity in the upper and lower layers of the atmospheric troposphere suggest an analysis of the vertical structures of the EEP composite. This allows us to simultaneously analyze the temporal evolution of several variables at different pressure levels.

3.2.1. Vertical Profile around Yref 0

Figure 11 represents the tropospheric evolution (between H-24 and H+18) of the

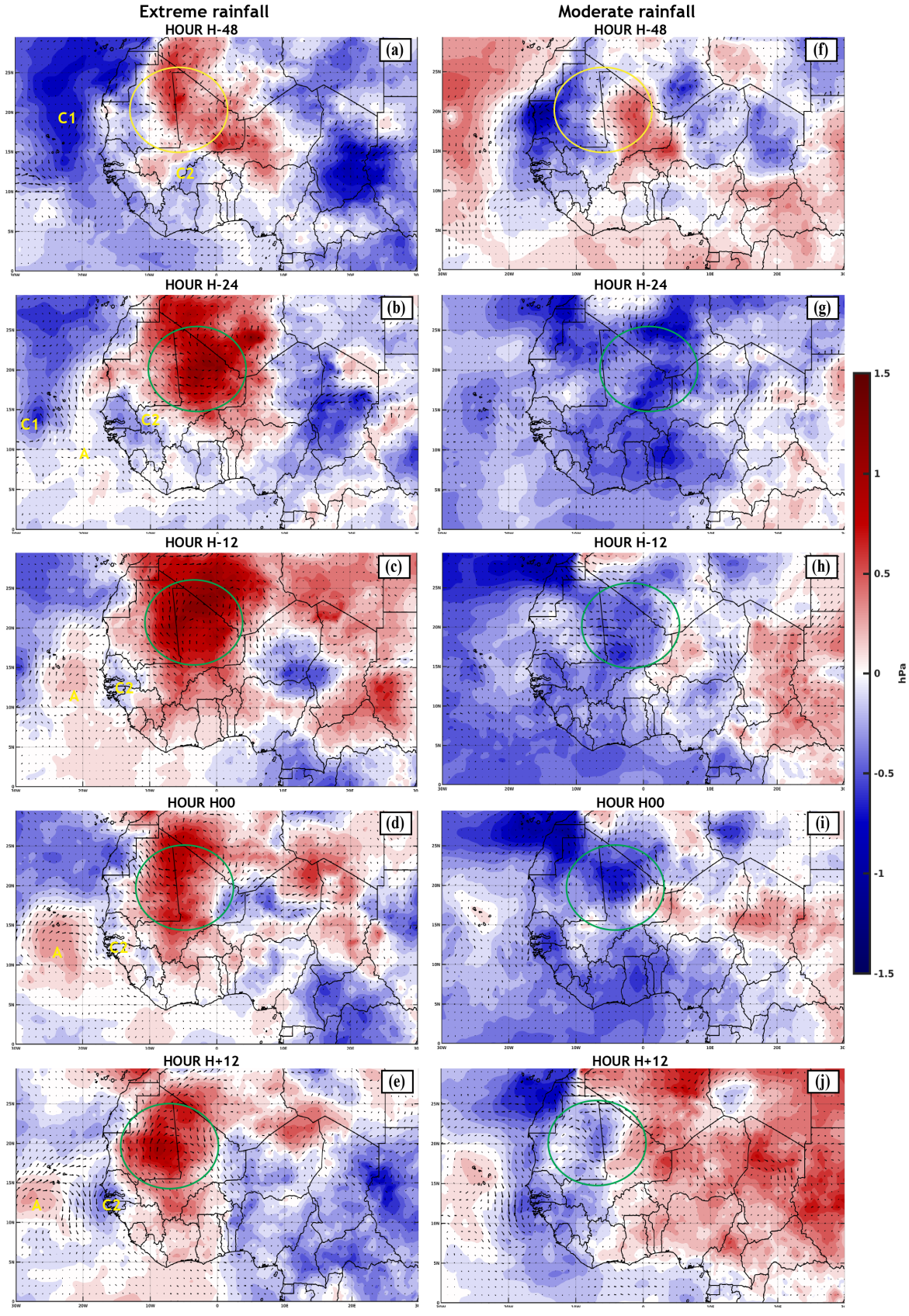

Figure 10. Anomalies of mean sea level pressure (color) and wind at 10 m (arrows).

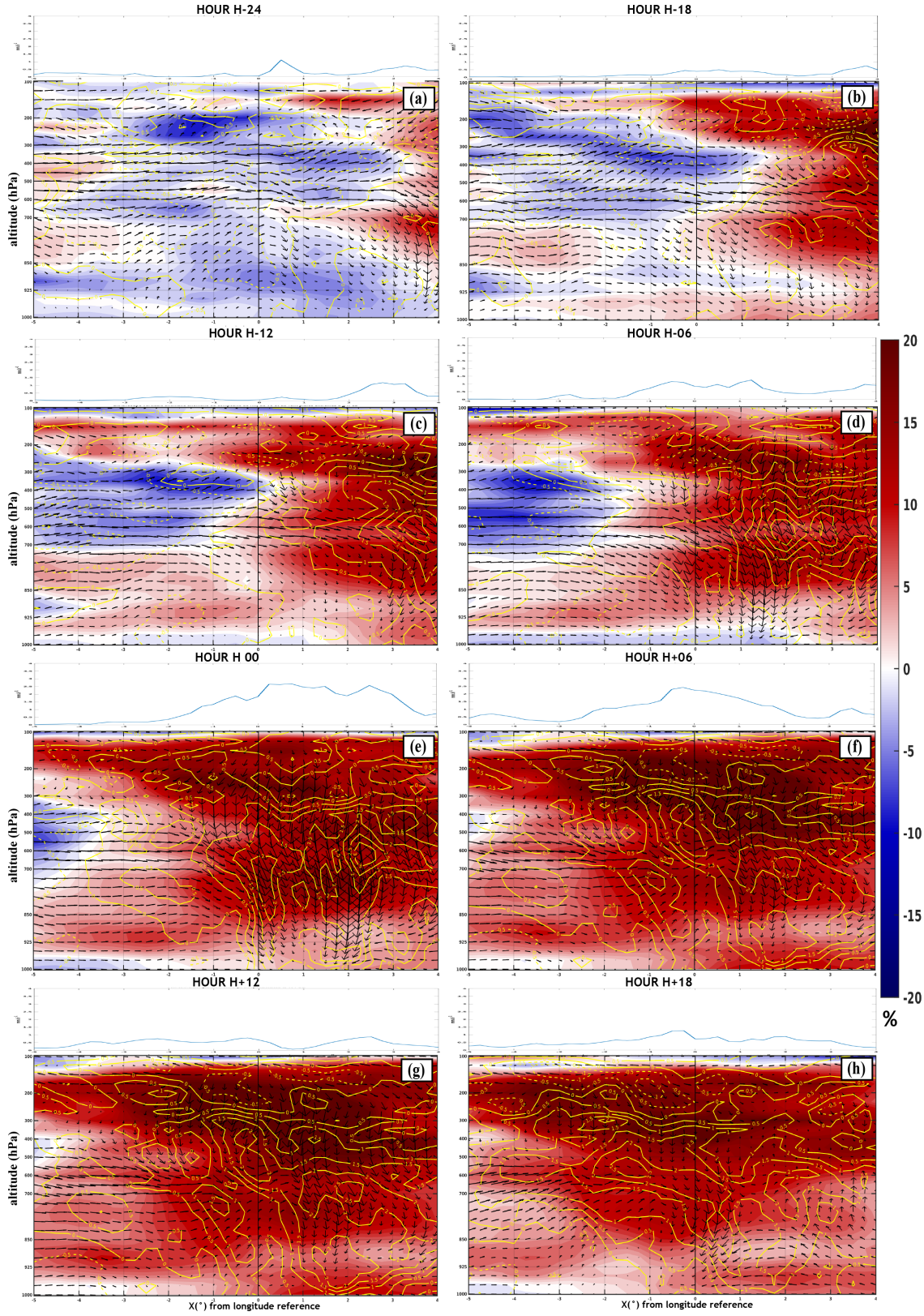

Figure 11. Vertical structures of anomalies of the relative humidity (color), relative vorticity (isoline) and wind (arrow). The evolution of precipitation with TRMM is represented by the blue curve. The vertical black line represents the reference longitude.

anomalies of relative humidity, relative vorticity and wind. On this same figure, the evolution of hourly precipitation intensity with TRMM is superimposed. The same reference abscissa as the vertical structure of the reanalyses is applied.

At H-24, negative anomalies of relative humidity and relative vorticity are observed from the surface up to 200-hPa around Xref 0. Between H-24 and H-18, a progressive increase in positive anomalies of relative humidity and relative vorticity to the east of Xref 0 is noted. These positive anomalies subsequently progress towards the West and reach the location of the composite of events between H-12 and H-6. It is between H+00 and H+06 where the maximum precipitation intensities are observed, that the entire tropospheric column is driven by strong relative humidity anomalies and their maxima (around 20%) are noted in the bands between 850 and 700-hPa and between 300 and 200-hPa.

The relative vorticity anomaly obtains its maximum value around 700-hPa. Around Xref 0, values between 1 and 1.5×10^{-5} s^{-1} are noted, however the maximum value (2.5×10^{-5} s^{-1}) corresponding to the center of the vortex is noted further to the East. Which shows us that the precipitating systems are located ahead of the wave trough.

Compared to the distribution of wind anomalies, the analysis shows descending and ascending currents but also an advection (convergence) in the low levels (surface-850 hPa) on both sides around Xref 0. At high altitude (around 200-hPa), a divergence of the wind anomaly accompanies the area of maximum relative humidity is present. This configuration implies the presence of a well-structured convective system with the direction of the anvil flow.

The AEJ partly modulates the development and organization of precipitation. In return, precipitation acts on the AEJ since it modifies surface temperature and humidity (Nicholson & Grist, 2003). At pressure levels where we can follow the AEJ (between 600 and 700-hPa), the wind anomalies from the West throughout the process. This could correspond to a weakening of the intensity of the AEJ.

3.2.2. Vertical Profile around Xref 0 and Yref 0

Knowing that previous analyzes on rain extremes showed a strong presence of humidity and the transition from an AEW to Xref 0, a tropospheric analysis as a function of time (between H-72 and H+72) is carried out at using **Figure 12**. Comparing the relative humidity and relative vorticity structures for extreme rain (**Figure 12(a)**) and moderate rain (**Figure 12(b)**) shows a large difference in terms of configuration. For rain extremes, the vertical extension of relative humidity is more marked in the low layers as well as in the upper tropospheric layers with maximum values obtained between H+00 and H+06 reaching more than 90%. Concerning moderate rainfall, the moisture content is also quite high in the lower layers even if it is lower than that of extreme rainfall. In the middle and upper layers, the content is quite low compared to the extremes of rain. This difference in configuration in terms of humidity between these two types of precipitation also manifests itself with the relative vorticity. Its maximum values are 3×10^{-5} s^{-1} for extreme rainfall and 1×10^{-5} s^{-1} for moderate rainfall.

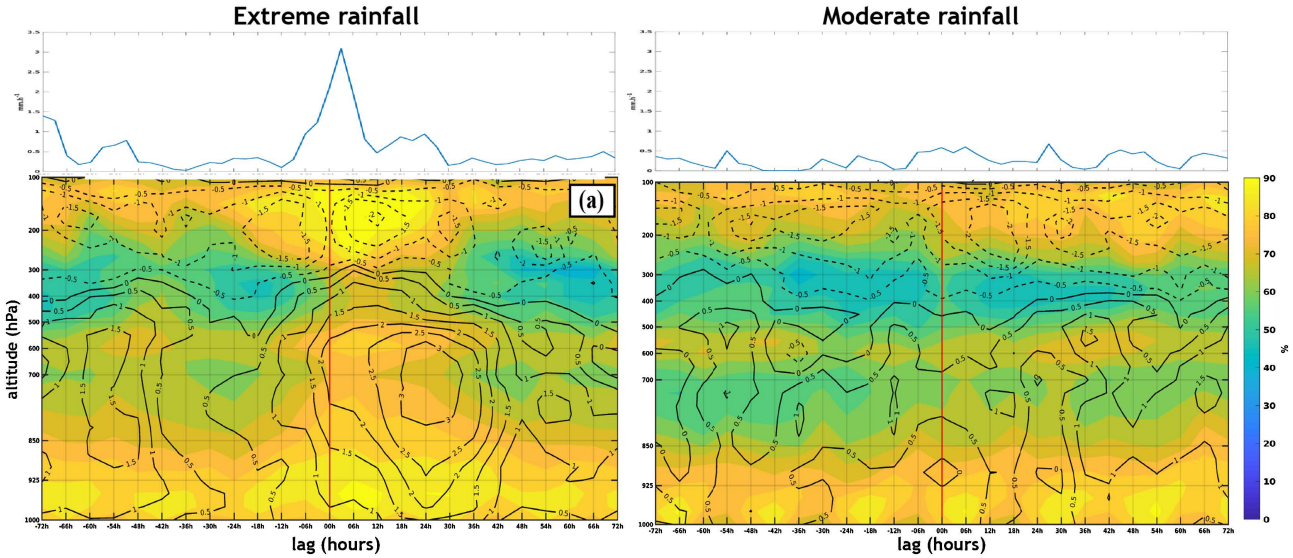

Figure 12. Vertical structures of relative humidity (color) and relative vorticity (isoline) for extremes of rainfall (a) and for moderate rainfall (b). The evolution of precipitation with TRMM is represented by the blue curve. The vertical red line represents the reference time.

The analysis of **Figure 13(a)** shows the presence of a strong positive humidity anomaly between H-12 and H+30 with significant values. These anomalies are mainly marked in the middle and upper layers between H+00 and H+06 with 15% between 700 and 850-hPa. The anomaly maximum of 20% is located in the interval between 200 and 300-hPa.

The southern wind anomaly represented by **Figure 13(b)** indicates the passage of the wave trough around H+18 with the alternation of the passage from the North wind to the South wind. A northerly wind dominates from the surface until around 300-hPa for the time interval between H-24 and H+06, thus covering the time of extreme rains.

Figure 13(c) shows the zonal wind anomalies. It tells us, in the middle layers, a positive anomaly presents between H-72 and H+30 with a maximum between H-18 and H+00 (2 $m \cdot s^{-1}$). This anomaly results in a significant weakening of the intensity of the AEJ. Configuration that may correspond to convective activity on the one hand, and on the other hand by the effect of the strong vorticity of the wind at 700-hPa with a dominant southern component.

3.3. Statistics of Variables

Knowing that the rain extremes studied are closely linked and modulated by the AEW, a statistical analysis of the composite of several atmospheric parameters is carried out. **Figure 14** shows the Hovmoller diagrams of the composites of relative vorticity and meridional wind at 700 and 850-hPa, and zonal wind at 700-hPa.

The relative vorticity at 700 (**Figure 14(a)**) gives the passage of two wave troughs around Xref 0. The first trough (T1) makes its passage on the 2 to 3 days before the extreme rain, and the second (T2) from the DD with an average speed of 6.17 $m \cdot s^{-1}$.

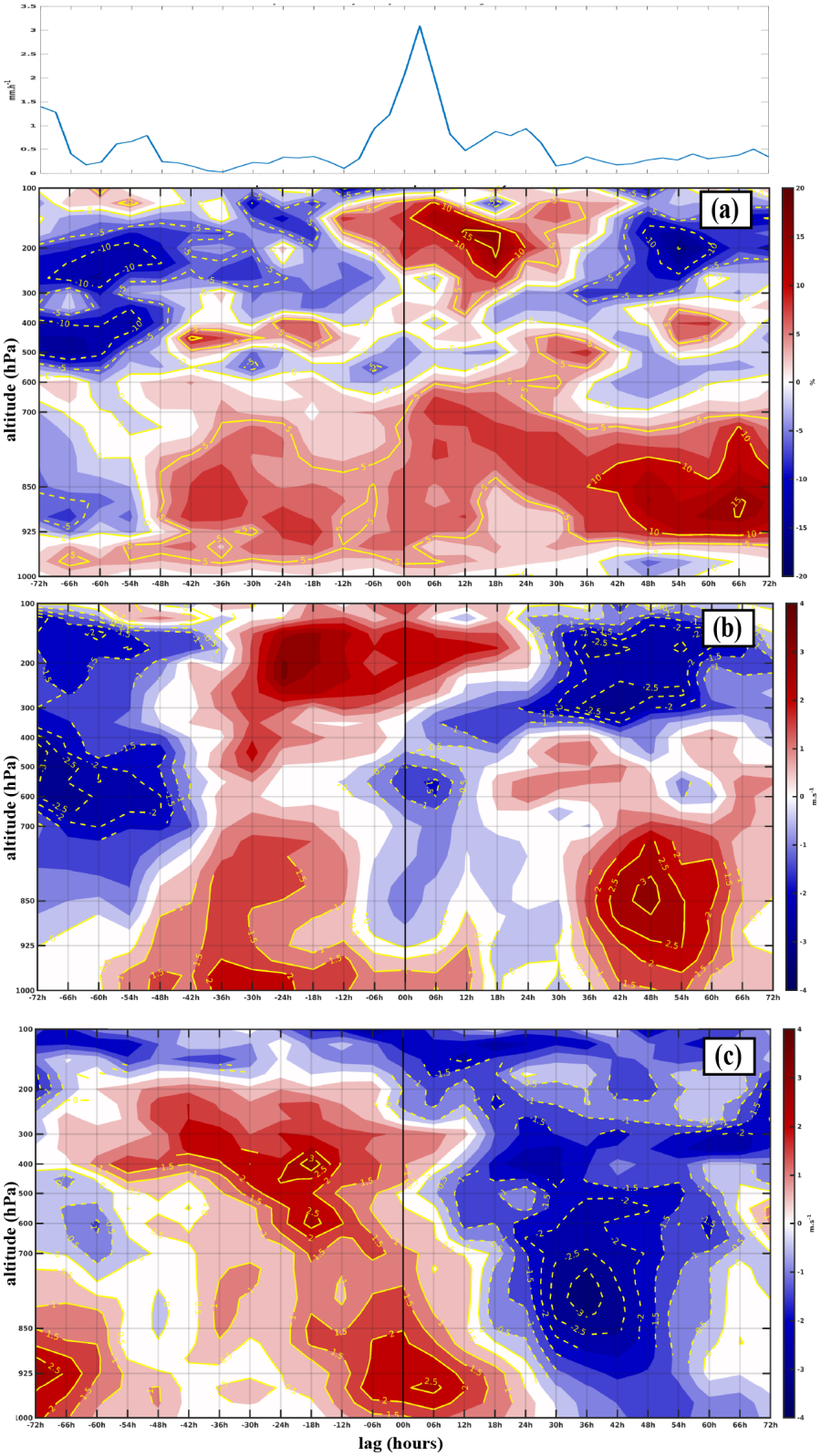

Figure 13. Vertical structures of the anomalies of relative humidity (a), meridional wind (b) and zonal wind (c) and their significance (isolines) with ERA5. The evolution of precipitation with TRMM is represented by the blue curve. The vertical black line represents the reference time.

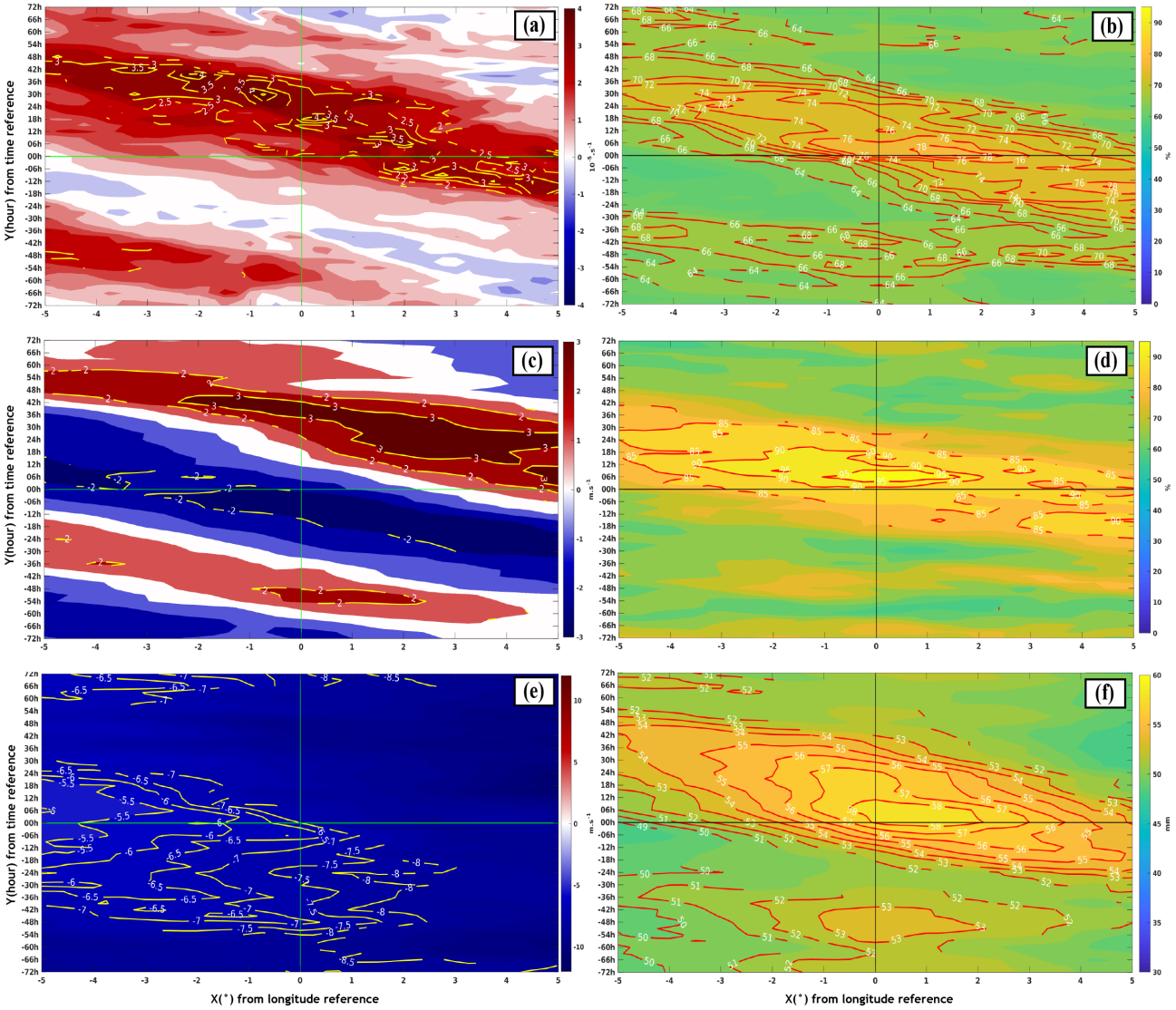

Figure 14. Hovmoller diagram of the composite of the relative vorticity (a), the meridional wind (c) and the zonal wind (e) at 700-hPa. The relative humidity at 700-hPa (b) and 200-hPa (d), and the precipitable water (f). The Monte Carlo significance test is applied for each variable (isoline). The vertical green line is the reference longitude and the horizontal green line is the reference time for the start of precipitation.

An analysis of the southern wind at 700-hPa is then carried out in order to see their spatio-temporal evolutions. Figure 14(c) shows an alternation of successive passages around Xref 0 of two pairs of winds from different directions. Each of these pairs of winds is composed of a north wind followed by a south wind. The first pair corresponds to the passage of the first wave trough detected between H-72 and H-48 and the second pair corresponds to the wave trough which is the main source of energy (T2) of significant precipitation noted from H00. We note that a northerly wind is present at the time of the event, which implies that the precipitating system is ahead of the trough in relation to the direction of its movement (East to West).

The analysis of the zonal wind at 700-hPa confirms the release of AEJ shear

(Figure 14(e)) with significantly low values between H-54 and H+06 with an average speed of 7 $m \cdot s^{-1}$ around Xref 0. However, we note a slight increase of 0.5 $m \cdot s^{-1}$ (i.e. 7.5 $m \cdot s^{-1)}$ around H-24.

AEWs are sources of energy and are linked to the advection of moisture in the troposphere. The composite analysis of relative humidity at 700-hPa (Figure 14(b)) shows the same configurations as the relative vorticity with two significant humidity waves around Xref 0. However, the larger values are obtained from H00. The minimum significance threshold at 700-hPa is 64% and the maximum noted from the start of the extreme rains with value of 78%.

Concerning the relative humidity at 200-hPa (Figure 14(d)), unlike the pressure level of 700-hPa, significance is only obtained from H00. The minimum significance threshold is 85% and a maximum of 95%.

Analyzes of relative humidity over several tropospheric pressure levels showed significant values, so an analysis of the composite of precipitable water over the entire air column is made. Figure 14(f) indicates significance between H-72 and H-48 with a maximum value of 53 $Kg \cdot m^{-2}$. However, we note from H00 the maximum of 58 $Kg \cdot m^{-2}$. The threshold significance value is 50 $Kg \cdot m^{-2}$.

4. Conclusion

The objective of this study was to study the dynamics of atmospheric conditions associated with extreme rain events listed in the database of the Directorate of Civil Protection of Senegal (DPC) and significant socio-economic impacts that they have caused. An original analysis of the composite of the 17 most extreme events was carried out on the synoptic and large scales. For this, TRMM satellite observation data were used to analyze the spatio-temporal location of precipitation. The atmospheric reanalyses of ERA5 made it possible to see the behavior of certain atmospheric parameters, mainly in the time interval between H-72 and H+72, for the composite of rain extremes. A comparative analysis against the configuration of the composite of moderate rain events was also carried out.

The results of the analyzes of the different atmospheric parameters studied show, on the synoptic scale, that extreme rain events are mainly modulated by AEWs. Rainfall extremes are characterized by high vorticity values unlike moderate rainfall. These strong vorticity anomalies are mainly characterized by two troughs and a ridge. These anomalies created disturbances in the wind field at 700-hPa and these had an influence on the trajectory of the AEJ and caused, in part, a weakening of the jet.

Strong convergences of moisture transport, in the lower tropospheric layers, due to these vortices are recorded. The humidity anomalies are more marked to the North of the western Sahel because the ridge (A), which is located behind the first cyclonic circulation (C1), has advected a lot of humidity from the sea towards the continental North. The second cyclonic circulation (C2), accompanying the MCS causing extreme rainfall, also advected moisture from off the Guinean coast.

At altitude around 200-hPa, a response of this convergence of humidity in the

low levels accompanied by the vertical transport of humidity is highlighted by strong anomalies as well as a divergence of the winds. This configuration indicates the presence of a well-structured convective system vertically.

The position of the SHL influences the direction of moisture flux transport and in comparison, with the EPM, the position of the SHL of the EEP is slightly further west. However, the Saharan depression is less intense with the EEP and a positive surface pressure anomaly is noted. Then the intensity of the SHL might not play an important role in the intensity of the moisture flux at the continental level. The presence of high humidity values is, in large part, attributed to the passage of the wave with the arrangement of its vortices and the surface depression below the precipitating system.

The analysis of relative vorticity, wind, relative humidity as well as precipitable water shows that they are good indicators for characterizing rain extremes. The behavior of the anomalies of these variables shows the presence of a significant amount of humidity in the tropospheric column and the most marked pressure levels are between 850 and 700-hPa and in the upper layers around 200-hPa.

In statistical terms, the main variables observed give, for the most part, significant values with the Monte-Carlo test between H-72 and H-48. However, the highest significant values are obtained from H00, thus accompanying the extremes of rainfall.

Initially dry regions that have been watered may be particularly conducive to triggering deep convection in the following 2 - 3 days (Taylor, et al., 2011b). Therefore, the presence of precipitation, around Xref 0, between H-72 and H-48 before the arrival of extreme rains from H00, could play an important role in surface conditions in terms of moisture supply. However, Taylor, Parker, et al., 2011a showed that surface heterogeneities can help initiate convection, but they appear to play a secondary role when an AEW is already formed. Nevertheless, this arouses particular interest in carrying out a study on the influence of these surface heterogeneities on the development of MCS having caused extremes of rainfall. It would also be interesting to study the relationship between easterly wave activity, extreme rain events and the initiation of tropical cyclones at ocean level.

Conflicts of Interest

The authors declare no conflicts of interest regarding the publication of this paper.

References

Bain, C. L., Williams, K. D., Milton, S. F., & Heming, J. T. (2014). Objective Tracking of African Easterly Waves in Met Office Models. *Quarterly Journal of the Royal Meteorological Society, 140,* 47-57. https://doi.org/10.1002/qj.2110

Bell, M. A., & Lamb, P. J. (2006). Integration of Weather System Variability to Multidecadal Regional Climate Change: The West African Sudan-Sahel Zone, 1951-98. *Journal of Climate, 19,* 5343-5365. https://doi.org/10.1175/jcli4020.1

Berry, G. J., & Thorncroft, C. D. (2012). African Easterly Wave Dynamics in a Mesoscale Numerical Model: The Upscale Role of Convection. *Journal of the Atmospheric*

Sciences, 69, 1267-1283. https://doi.org/10.1175/jas-d-11-099.1

Berry, G., Thorncroft, C., & Hewson, T. (2007). African Easterly Waves during 2004—Analysis Using Objective Techniques. *Monthly Weather Review, 135,* 1251-1267. https://doi.org/10.1175/mwr3343.1

Carlson, T. N. (1969a). Some Remarks on African Disturbances and Their Progress Over the Tropical Atlantic. *Monthly Weather Review, 97,* 716-726. https://doi.org/10.1175/1520-0493(1969)097<0716:sroada>2.3.co;2

Carlson, T. N. (1969b). Synoptic Histories of Three African Disturbances That Developed into Atlantic Hurricanes. *Monthly Weather Review, 97,* 256-276. https://doi.org/10.1175/1520-0493(1969)097<0256:shotad>2.3.co;2

Cornforth, R., Mumba, Z., Parker, D. J., Berry, G., Chapelon, N., Diakaria, K. et al. (2017). Synoptic Systems. In D. J. Parker, & M. Diop-Kane (Eds.), *Meteorology of Tropical West Africa: The Forecasters' Handbook* (pp. 40-89). John Wiley & Sons, Ltd. https://doi.org/10.1002/9781118391297.ch2

Crétat, J., Vizy, E. K., & Cook, K. H. (2015). The Relationship between African Easterly Waves and Daily Rainfall over West Africa: Observations and Regional Climate Simulations. *Climate Dynamics, 44,* 385-404. https://doi.org/10.1007/s00382-014-2120-x

Dai, A., Trenberth, K. E., & Qian, T. (2004). A Global Dataset of Palmer Drought Severity Index for 1870-2002: Relationship with Soil Moisture and Effects of Surface Warming. *Journal of Hydrometeorology, 5,* 1117-1130. https://doi.org/10.1175/jhm-386.1

Descroix, L., Diongue Niang, A., Panthou, G., Bodian, A., Sane, Y., Dacosta, H. et al. (2016). Évolution récente de la pluviométrie en Afrique de l'ouest à travers deux régions: La Sénégambie et le bassin du Niger moyen. *Climatologie, 12,* 25-43. https://doi.org/10.4267/climatologie.1105

Diedhiou, A., Janicot, S., Viltard, A., de Felice, P., & Laurent, H. (1999). Easterly Wave Regimes and Associated Convection over West Africa and Tropical Atlantic: Results from the NCEP/NCAR and ECMWF Reanalyses. *Climate Dynamics, 15,* 795-822. https://doi.org/10.1007/s003820050316

Douglas, I., Alam, K., Maghenda, M., Mcdonnell, Y., Mclean, L., & Campbell, J. (2008). Unjust Waters: Climate Change, Flooding and the Urban Poor in Africa. *Environment and Urbanization, 20,* 187-205. https://doi.org/10.1177/0956247808089156

Engel, T., Fink, A. H., Knippertz, P., Pante, G., & Bliefernicht, J. (2017). Extreme Precipitation in the West African Cities of Dakar and Ouagadougou: Atmospheric Dynamics and Implications for Flood Risk Assessments. *Journal of Hydrometeorology, 18,* 2937-2957. https://doi.org/10.1175/jhm-d-16-0218.1

Fall, M., Dieng, A. L., Sall, S. M., Sane, Y., & Diakhaté, M. (2020). Synoptic Analysis of Extreme Rainfall Event in West Africa: The Case of Linguère. *American Journal of Environmental Protection, 8,* 1-9.

Fink, A. H., & Reiner, A. (2003). Spatiotemporal Variability of the Relation between African Easterly Waves and West African Squall Lines in 1998 and 1999. *Journal of Geophysical Research: Atmospheres, 108,* 1-17. https://doi.org/10.1029/2002jd002816

Fink, A. H., Vincent, D. G., & Ermert, V. (2006). Rainfall Types in the West African Sudanian Zone during the Summer Monsoon 2002. *Monthly Weather Review, 134,* 2143-2164. https://doi.org/10.1175/mwr3182.1

Gallego, D., Ordóñez, P., Ribera, P., Peña-Ortiz, C., & García-Herrera, R. (2015). An Instrumental Index of the West African Monsoon Back to the Nineteenth Century. *Quarterly Journal of the Royal Meteorological Society, 141,* 3166-3176.

https://doi.org/10.1002/qj.2601

Hardoy, J. E., Mitlin, D., & Satterthwaite, D. (2001). Environmental Problems in an Urbanizing World: Finding Solutions for Cities in Africa, Asia and Latin America. Routledge. https://doi.org/10.4324/9781315071732

Hartill, L. (2008). Understanding West Africa's Rising Food Prices. https://reliefweb.int/report/burkina-faso/understanding-west-africas-rising-food-prices

Hastenrath, S. (1999). Dynamics of the Pacific Equatorial Dry Zone. *Meteorology and Atmospheric Physics, 71,* 243-254. https://doi.org/10.1007/s007030050058

Hersbach, H., Bell, B., Berrisford, P., Hirahara, S., Horányi, A., Muñoz-Sabater, J. et al. (2020). The ERA5 Global Reanalysis. *Quarterly Journal of the Royal Meteorological Society, 146,* 1999-2049. https://doi.org/10.1002/qj.3803

Huffman, G. J., Bolvin, D. T., Nelkin, E. J., Wolff, D. B., Adler, R. F., Gu, G. et al. (2007). The TRMM Multisatellite Precipitation Analysis (TMPA): Quasi-Global, Multiyear, Combined-Sensor Precipitation Estimates at Fine Scales. *Journal of Hydrometeorology, 8,* 38-55. https://doi.org/10.1175/jhm560.1

Hulme, M., Doherty, R., Ngara, T., New, M., & Lister, D. (2001). African Climate Change: 1900-2100. *Climate Research, 17,* 145-168. https://doi.org/10.3354/cr017145

Janicot, S. (1992a). Spatiotemporal Variability of West African Rainfall. Part I: Regionalizations and Typings. *Journal of Climate, 5,* 489-497. https://doi.org/10.1175/1520-0442(1992)005<0489:svowar>2.0.co;2

Janicot, S. (1992b). Spatiotemporal Variability of West African Rainfall. Part II: Associated Surface and Airmass Characteristics. *Journal of Climate, 5,* 499-511. https://doi.org/10.1175/1520-0442(1992)005<0499:svowar>2.0.co;2

Joyce, R., Janowiak, J., & Huffman, G. (2001). Latitudinally and Seasonally Dependent Zenith-Angle Corrections for Geostationary Satellite IR Brightness Temperatures. *Journal of Applied Meteorology, 40,* 689-703. https://doi.org/10.1175/1520-0450(2001)040<0689:lasdza>2.0.co;2

Kiladis, G. N., Thorncroft, C. D., & Hall, N. M. J. (2006). Three-Dimensional Structure and Dynamics of African Easterly Waves. Part I: Observations. *Journal of the Atmospheric Sciences, 63,* 2212-2230. https://doi.org/10.1175/jas3741.1

Lafore, J., Beucher, F., Peyrillé, P., Diongue-Niang, A., Chapelon, N., Bouniol, D. et al. (2017). A Multi-Scale Analysis of the Extreme Rain Event of Ouagadougou in 2009. *Quarterly Journal of the Royal Meteorological Society, 143,* 3094-3109. https://doi.org/10.1002/qj.3165

Lamb, P. J. (1978a). Case Studies of Tropical Atlantic Surface Circulation Patterns during Recent Sub-Saharan Weather Anomalies: 1967 and 1968. *Monthly Weather Review, 106,* 482-491. https://doi.org/10.1175/1520-0493(1978)106<0482:csotas>2.0.co;2

Lamb, P. J. (1978b). Large-Scale Tropical Atlantic Surface Circulation Patterns Associated with Subsaharan Weather Anomalies. *Tellus A: Dynamic Meteorology and Oceanography, 30,* 240-251. https://doi.org/10.3402/tellusa.v30i3.10338

Lavaysse, C., Flamant, C., Janicot, S., Parker, D. J., Lafore, J.-P., Sultan, B. et al. (2009). Seasonal Evolution of the West African Heat Low: A Climatological Perspective. *Climate Dynamics, 33,* 313-330. https://doi.org/10.1007/s00382-009-0553-4

Le Barbé, L., Lebel, T., & Tapsoba, D. (2002). Rainfall Variability in West Africa during the Years 1950-90. *Journal of Climate, 15,* 187-202. https://doi.org/10.1175/1520-0442(2002)015<0187:rviwad>2.0.co;2

Lebel, T., & Ali, A. (2009). Recent Trends in the Central and Western Sahel Rainfall Regime (1990-2007). *Journal of Hydrology, 375,* 52-64.

https://doi.org/10.1016/j.jhydrol.2008.11.030

Lebel, T., Diedhiou, A., & Laurent, H. (2003). Seasonal Cycle and Interannual Variability of the Sahelian Rainfall at Hydrological Scales. *Journal of Geophysical Research: Atmospheres, 108,* 1-11. https://doi.org/10.1029/2001jd001580

Maggioni, V., Meyers, P. C., & Robinson, M. D. (2016). A Review of Merged High-Resolution Satellite Precipitation Product Accuracy during the Tropical Rainfall Measuring Mission (TRMM) Era. *Journal of Hydrometeorology, 17,* 1101-1117. https://doi.org/10.1175/jhm-d-15-0190.1

Ly, M., Traore, S. B., Alhassane, A., & Sarr, B. (2013). Evolution of Some Observed Climate Extremes in the West African Sahel. *Weather and Climate Extremes, 1,* 19-25. https://doi.org/10.1016/j.wace.2013.07.005

Nchito, W. S. (2007). Flood Risk in Unplanned Settlements in Lusaka. *Environment and Urbanization, 19,* 539-551. https://doi.org/10.1177/0956247807082835

Nicholson, S. E., & Grist, J. P. (2003). The Seasonal Evolution of the Atmospheric Circulation over West Africa and Equatorial Africa. *Journal of Climate, 16,* 1013-1030. https://doi.org/10.1175/1520-0442(2003)016<1013:tseota>2.0.co;2

Nicholson, S. E., Some, B., McCollum, J., Nelkin, E., Klotter, D., Berte, Y. et al. (2003). Validation of TRMM and Other Rainfall Estimates with a High-Density Gauge Dataset for West Africa. Part I: Validation of GPCC Rainfall Product and Pre-TRMM Satellite and Blended Products. *Journal of Applied Meteorology, 42,* 1337-1354. https://doi.org/10.1175/1520-0450(2003)042<1337:votaor>2.0.co;2

Panthou, G., Lebel, T., Vischel, T., Quantin, G., Sane, Y., Ba, A. et al. (2018). Rainfall Intensification in Tropical Semi-Arid Regions: The Sahelian Case. *Environmental Research Letters, 13,* Article 064013. https://doi.org/10.1088/1748-9326/aac334

Panthou, G., Vischel, T., & Lebel, T. (2014). Recent Trends in the Regime of Extreme Rainfall in the Central Sahel. *International Journal of Climatology, 34,* 3998-4006. https://doi.org/10.1002/joc.3984

Payne, S. W., & McGarry, M. M. (1977). The Relationship of Satellite Inferred Convective Activity to Easterly Waves over West Africa and the Adjacent Ocean during Phase III of Gate. *Monthly Weather Review, 105,* 413-420. https://doi.org/10.1175/1520-0493(1977)105<0413:trosic>2.0.co;2

Poan, D. E., Lafore, J., Roehrig, R., & Couvreux, F. (2015). Internal Processes within the African Easterly Wave System. *Quarterly Journal of the Royal Meteorological Society, 141,* 1121-1136. https://doi.org/10.1002/qj.2420

Prakash, S., Mitra, A. K., Momin, I. M., Pai, D. S., Rajagopal, E. N., & Basu, S. (2015). Comparison of TMPA-3B42 Versions 6 and 7 Precipitation Products with Gauge-Based Data over India for the Southwest Monsoon Period. *Journal of Hydrometeorology, 16,* 346-362. https://doi.org/10.1175/jhm-d-14-0024.1

Reed, R. J., Norquist, D. C., & Recker, E. E. (1977). The Structure and Properties of African Wave Disturbances as Observed during Phase III of Gate. *Monthly Weather Review, 105,* 317-333. https://doi.org/10.1175/1520-0493(1977)105<0317:tsapoa>2.0.co;2

Salack, S., Klein, C., Giannini, A., Sarr, B., Worou, O. N., Belko, N. et al. (2016). Global Warming Induced Hybrid Rainy Seasons in the Sahel. *Environmental Research Letters, 11,* Article 104008. https://doi.org/10.1088/1748-9326/11/10/104008

Salack, S., Muller, B., & Gaye, A. T. (2011). Rain-Based Factors of High Agricultural Impacts over Senegal. Part I: Integration of Local to Sub-Regional Trends and Variability. *Theoretical and Applied Climatology, 106,* 1-22. https://doi.org/10.1007/s00704-011-0414-z

Sanogo, S., Fink, A. H., Omotosho, J. A., Ba, A., Redl, R., & Ermert, V. (2015). Spatio-Temporal Characteristics of the Recent Rainfall Recovery in West Africa. *International Journal of Climatology, 35,* 4589-4605. https://doi.org/10.1002/joc.4309

Schwendike, J., & Jones, S. C. (2010). Convection in an African Easterly Wave over West Africa and the Eastern Atlantic: A Model Case Study of *Helene* (2006). *Quarterly Journal of the Royal Meteorological Society, 136,* 364-396. https://doi.org/10.1002/qj.566

Siongco, A. C., Hohenegger, C., & Stevens, B. (2015). The Atlantic ITCZ Bias in CMIP5 Models. *Climate Dynamics, 45,* 1169-1180. https://doi.org/10.1007/s00382-014-2366-3

Taylor, C. M., Belušić, D., Guichard, F., Parker, D. J., Vischel, T., Bock, O. et al. (2017). Frequency of Extreme Sahelian Storms Tripled since 1982 in Satellite Observations. *Nature, 544,* 475-478. https://doi.org/10.1038/nature22069

Taylor, C. M., Gounou, A., Guichard, F., Harris, P. P., Ellis, R. J., Couvreux, F. et al. (2011b). Frequency of Sahelian Storm Initiation Enhanced over Mesoscale Soil-Moisture Patterns. *Nature Geoscience, 4,* 430-433. https://doi.org/10.1038/ngeo1173

Taylor, C. M., Parker, D. J., Kalthoff, N., Gaertner, M. A., Philippon, N., Bastin, S. et al. (2011a). New Perspectives on Land-Atmosphere Feedbacks from the African Monsoon Multidisciplinary Analysis. *Atmospheric Science Letters, 12,* 38-44. https://doi.org/10.1002/asl.336

Vischel, T., Panthou, G., Peyrillé, P., Roehrig, R., Quantin, G., Lebel, T. et al. (2019). Precipitation Extremes in the West African Sahel. In V. Venugopal, J. Sukhatme, R. Murtugudde, & R. Roca Eds., *Tropical Extremes: Natural Variability and Trends* (pp. 95-138). Elsevier. https://doi.org/10.1016/b978-0-12-809248-4.00004-2

Vizy, E. K., & Cook, K. H. (2022). Distribution of Extreme Rainfall Events and Their Environmental Controls in the West African Sahel and Soudan. *Climate Dynamics, 59,* 997-1026. https://doi.org/10.1007/s00382-022-06171-x

Vizy, E. K., & Cook, K. H. (2024). Understanding Extreme Rainfall in the Sahel of Southwestern Mali. *Climate Dynamics, 62,* 1-25. https://doi.org/10.1007/s00382-024-07241-y

Wang, C., Zhang, L., Lee, S., Wu, L., & Mechoso, C. R. (2014). A Global Perspective on CMIP5 Climate Model Biases. *Nature Climate Change, 4,* 201-205. https://doi.org/10.1038/nclimate2118

Wilcox, C., Vischel, T., Panthou, G., Bodian, A., Blanchet, J., Descroix, L. et al. (2018). Trends in Hydrological Extremes in the Senegal and Niger Rivers. *Journal of Hydrology, 566,* 531-545. https://doi.org/10.1016/j.jhydrol.2018.07.063

Zhang, C., Woodworth, P., & Gu, G. (2006). The Seasonal Cycle in the Lower Troposphere over West Africa from Sounding Observations. *Quarterly Journal of the Royal Meteorological Society, 132,* 2559-2582. https://doi.org/10.1256/qj.06.23

Zulkafli, Z., Buytaert, W., Onof, C., Manz, B., Tarnavsky, E., Lavado, W. et al. (2014). A Comparative Performance Analysis of TRMM 3B42 (TMPA) Versions 6 and 7 for Hydrological Applications over Andean-Amazon River Basins. *Journal of Hydrometeorology, 15,* 581-592. https://doi.org/10.1175/jhm-d-13-094.1